

Quantitative Restoration for MODIS Band 6 on Aqua

Irina Gladkova, Michael D. Grossberg, Fazlul Shahriar, George Bonev, and Peter Romanov

Abstract—Due to the harsh conditions of space, the detectors within satellite-based multispectral imagers are always at risk of damage or failure. In particular, 15 out of the 20 detectors that produce the 1.6- μm band 6 of Moderate Resolution Imaging Spectroradiometer (MODIS) on Aqua are either dead or noisy. In this paper, we describe a quantitative image restoration (QIR) algorithm that is able to accurately estimate and restore the data lost due to multiple-detector failure. The small number of functioning detectors is used to train a restoration function that is based on a multivariate regression using the information in a spatial-spectral window around each restored pixel. The information from other spectral bands allows QIR to perform well even when standard image interpolation breaks down due to large contiguous sections of the image being missing, as is the case for MODIS band 6 on Aqua. We present a comprehensive evaluation of the QIR algorithm by simulating the Aqua damage using the working 1.6- μm band of MODIS on Terra and then comparing the QIR restoration to the original (unbroken) Terra image. We also compare our results with other researchers' prior work that has been based on the assumption that band 6 could be approximated well solely as a function of the related band 7. We present empirical evidence that there is information in the other 500- and 250-m bands, excluding bands 6 and 7, that can inform the estimation of missing band 6 data. We demonstrate superior performance of QIR over previous algorithms as reflected by a reduced root-mean-square-error evaluation. The QIR algorithm may also be adapted to other cases and provides a powerful and general algorithm to mitigate the risks of detector damage in multispectral remote sensing.

Index Terms—Aqua, band 6, Moderate Resolution Imaging Spectroradiometer (MODIS), restoration, stripping.

I. INTRODUCTION

NEW understanding of the Earth's environment is increasingly dependent on multispectral satellite imager data. Potential system failures in an imager may result in the loss of these precious data. Typically, an imager collects the data via many sensitive detectors. The launch processes, deployment into the harsh environment of space, particle bombardment,

Manuscript received March 10, 2011; revised July 8, 2011; accepted October 9, 2011. Date of publication December 5, 2011; date of current version May 16, 2012. This work was supported in part by the Center for Satellite Applications and Research, National Environmental Satellite, Data, and Information Service, National Oceanic and Atmospheric Administration, under Grant DG133E07CQ0077. The views, opinions, and findings in this paper are those of the authors and should not be construed as an official NOAA and/or U.S. Government position, policy, or decision.

I. Gladkova, M. D. Grossberg, and P. Romanov are with the National Oceanic and Atmospheric Administration/Cooperative Remote Sensing Science and Technology Center, The City College of New York, The City University of New York, New York, NY 10031 USA (e-mail: gladkova@cs.cuny.cuny.edu; grossberg@cs.cuny.cuny.edu; Peter.Romanov@noaa.gov).

F. Shahriar and G. Bonev are with The Graduate Center, The City University of New York, New York, NY 10016 USA (e-mail: fshahriar@gc.cuny.edu; gbonev@gc.cuny.edu).

Color versions of one or more of the figures in this paper are available online at <http://ieeexplore.ieee.org>.

Digital Object Identifier 10.1109/TGRS.2011.2173499

and exposure to radiation and space dust can result in detector damage at any point in an imager's life cycle.

When a damaged detector produces noisy or distorted data in a scanning imager such as Moderate Resolution Imaging Spectroradiometer (MODIS), it results in periodic stripes. This is because, during every scan, the set of detectors produces a group of scanlines in the image. A single detector produces a single scanline, and as the groups of scanlines are built up to produce an image, the broken detectors produce periodic noisy or dropped lines which appear as stripes. Detector damage, and thus striping, is an unavoidable risk to remote sensing projects.

There are many examples of imagers that suffer from striping. Classical examples include Landsat 4 and 5, and a more recent example is the water vapor (WV) 6.2 band on the Spinning Enhanced Visible and Infrared Imager (SEVIRI). To deal with this problem, the European Organisation for the Exploitation of Meteorological Satellites developed an anomaly compensation algorithm designed to suppress visible stripes from occurring in two out of its three detectors for that band. That algorithm is guided by heuristic arguments and not generalizable because it is based around the specific problems with the WV 6.2 band on SEVIRI.

A particularly important example of periodic line drop is the 1.6- μm band in the MODIS instrument on the Aqua satellite of the National Aeronautics and Space Administration (NASA). Fifteen out of 20 detectors in this band are broken, meaning that their data are missing or so noisy as to be considered unusable [6], [7]. Currently, the data are published with the locations of missing data recorded in the metadata. In addition, NASA publishes band 6 with the missing scanlines filled in using columnwise linear interpolation. This simple interpolation method results in artifacts due to the significant data loss, and it sometimes even fills pixels with statistically or physically implausible image values.

Instead of simply filling in the missing data via interpolation, we propose that the missing values should be estimated statistically from all available information. More narrowly, we note that, for multispectral imagers, the other spectral bands often jointly contain enough information to accurately estimate the missing data. Our approach is based on the fact that, while individual channels may not share strong enough pairwise correlation with the missing band, nonlinear multivariate relationships can still be exploited to recover the missing pixel values. In this paper, we demonstrate this idea by presenting an algorithm for the restoration of band 6 MODIS/Aqua using data from other spectral bands within the same multispectral image (granule). We use a spatial-spectral (i.e., multiband) neighborhood of undamaged band 6 pixels to train a multilinear piecewise restoration function. With this restoration function, we can restore a missing pixel value from the values

in a surrounding spatial–spectral neighborhood. This approach preserves the statistical structure of the uncorrupted data and avoids the artifacts of simple interpolation.

This paper makes several novel contributions. First, we present a method for estimating the missing pixels of band 6 from MODIS/Aqua at 500-m resolution, extending the method first presented in [2]. This extended method differs from our prior work in that we now use information from the 250-m bands 1 and 2 in addition to the functioning 500-m bands. It also differs from prior work that estimates the missing value in band 6 from the corresponding pixel in band 7 [6], [7]. In contrast, the quantitative image restoration (QIR) algorithm exploits a local spatial neighborhood in all the 250- and 500-m channels.

In addition to presenting the algorithm, we demonstrate the superior performance of our algorithm compared to NASA's basic interpolation and two algorithms which estimate band 6 using band 7 alone, through a comprehensive evaluation using ground truth data from the undamaged MODIS/Terra.

II. RELATED WORK

The simplest approach to replacing missing data is data interpolation. Interpolation is most effective when restoring scattered isolated missing pixels of scenes at points where it can be assumed that no edges or fine details are present, but this assumption does not apply to band 6 MODIS/Aqua images because they often contain fine cloud and land structural detail. In addition, rather than the lost pixels being isolated, many contiguous lines have been dropped, leaving large gaps in the data. Because whole rows of data have been dropped, NASA publishes band 6 MODIS/Aqua with the missing data filled in through linear interpolation along columns. The problem with this method is that there is not enough information coming from the good 25% of the detectors to restore the missing data; thus, columnwise interpolation introduces significant artifacts. Because of these artifacts, the image is smoother along columns than along rows. Since the rowwise interpolation dramatically corrupts image gradients, the image is unusable for any algorithm that uses gradients as input, such as edge detectors. A more general issue is that pure mathematical interpolation methods are based on heuristic assumptions of how missing data should be filled in; without scientific validation of these assumptions, there is no guarantee that the filled-in data will be accurate.

A more appropriate approach is to treat restoring the missing data as an estimation problem. In [7], the authors exploit this by fitting, at good band 6 detectors, a cubic polynomial expressing the band 6 pixel values as a function of band 7. They then use this polynomial to fill in the missing values. They evaluate this approach using MODIS/Terra bands 6 and 7 as proxies for the MODIS/Aqua band 7 and damaged band 6. They show that, by using regression to find the polynomial coefficients, they obtain a restoration that is significantly better than basic interpolation. A weakness in this approach is that, given the complex spectral reflectances of materials, there is no true functional relationship between band 6 and band 7.

A local cubic regression approach was proposed by Rakwatin *et al.* [6]. This approach drops the unrealistically

strong assumption that a global relationship between bands 6 and 7 exists and instead assumes that this relationship is only true locally. Thus, they let the parameters of a functional relation between bands 6 and 7 to vary. To do this, they define a sliding window of pixels centered at the pixel to be filled in, and then, they use the working sensors of band 6, and the corresponding sensors of band 7 within the sliding window, to perform a locally varying cubic regression. This local regression is then applied to the band 7 data to restore the band 6 data at the damaged sensors. Each pixel is filled in using a cubic polynomial with a potentially different set of coefficients. Note that, although a window is used to find the coefficients of the polynomial regression, the input to the regression is just the band 7 value. In addition to allowing the regression to vary across the image, they also applied histogram matching to the radiances to further improve the consistency of the regression and simultaneously reduce striping artifacts.

The fundamental problem with any approach that uses band 7 alone to determine band 6 is that these bands behave differently depending on surface and cloud composition; thus, while there are special cases—such as generally uniform parts of the image—where a functional relationship between band 7 and band 6 may be approximately valid, it does not hold in general. Moreover, if it did, there would be little need for inclusion of band 6 in the MODIS imager. While a single pixel value at the corresponding point in band 7 alone cannot provide enough information to restore band 6, we argue that, through the use of multiple bands and a local window as input (not just to train coefficients), much more information is available with which to perform the restoration.

We note that there are a number of other methods to reconstruct missing pixel values from an image. For example, *digital image inpainting* is often used to describe a kind of interpolation where the regions of missing data are so large that traditional interpolation fails; the variational and partial-differential-equation-based methods fill in missing data by finding the solution to a differential equation constrained by values surrounding the missing region. Examples of these methods can be found in the works of Ballester *et al.* [8], Bertalmio *et al.* [9], and Chan *et al.* [10]. These methods work well when the hole is relatively small and surrounded by large-scale geometric structure; however, when the surroundings of the hole consist of stochastic textures, such methods tend to produce blurred restoration and not to reproduce the texture. They also do not work well when the available undamaged data are sparse, as it is in the case of band 6.

Another set of methods based on work in texture synthesis generates plausible values within a missing region by randomly sampling from a probability distribution estimated from regions where the texture is assumed to be similar [11], [12]. These methods are inappropriate in the case of band 6 because we do not know, *a priori*, the class of texture that should be filled in. In addition, the sparse lines in band 6 from the working detectors do not provide the continuous patches that these methods typically use for sampling. These methods also tend to fail on regions with large-scale geometric structures like a coastline, or cloud edges. Exemplar-based methods such as those by Criminisi *et al.* [13] and Efros and Freeman [14] search

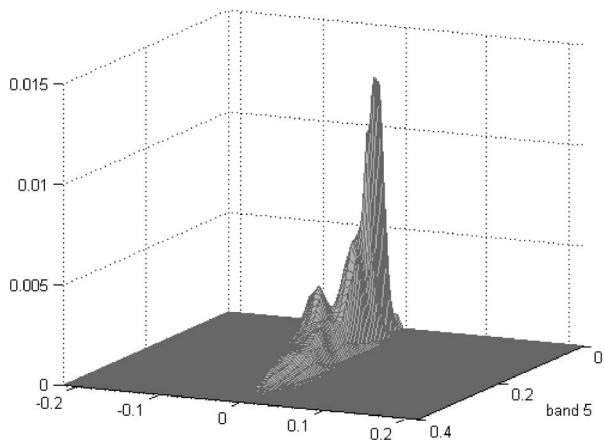


Fig. 1. Joint PDF of band 5 radiance and the residual of band 6 radiance with the portion predicted by band 7 subtracted.

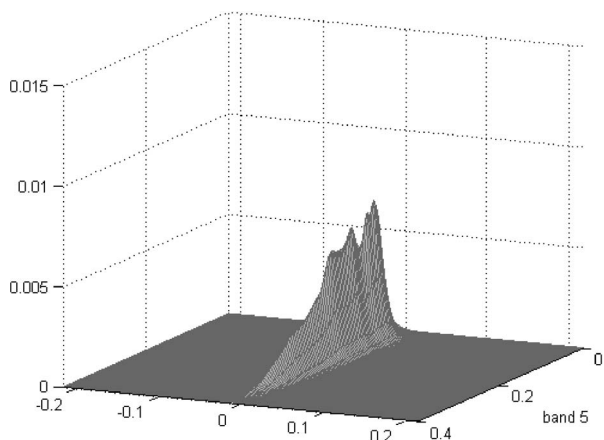


Fig. 2. Product of band 5 probability and residual of band 6 radiance with the portion predicted by band 7 subtracted.

for image patches which partially match pixels surrounding the hole but can be extended to cover the hole. These image patches are pasted in as filling for the missing pixels. Again, the sparse data available from the working detectors of channel 6 make this method inappropriate.

III. QIR ALGORITHM

As discussed previously, prior work has treated band 6 as a function of band 7. The general approach that we propose is to restore each missing pixel value in the damaged band using values taken from a spectral–spatial window, composed of all the nearby bands around that pixel. By introducing more variables, we can potentially improve our estimation if the new variables provide new information. In order to show that the new variable from band 5 provides additional information over that provided by band 7, we estimate the band 6 value using a cubic polynomial as in [7]. The difference between this estimated band 6 value and the actual band 6 value, which we call *radiance error*, is the part of the band 6 value not explained by band 7. The joint probability distribution of band 5 with the radiance error from band-7-estimated band 6 is shown in Fig. 1. If band 5 were *not* informative about this error, then the distribution would be independent, i.e., it would be the product of the single variable distributions, shown in Fig. 2. The

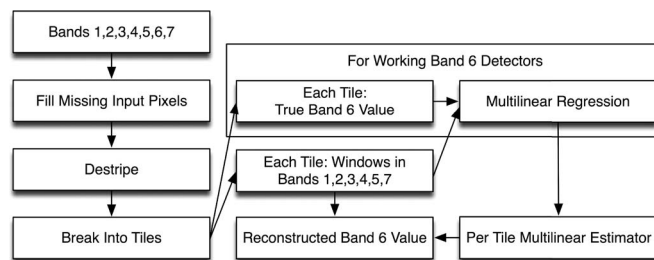


Fig. 3. Block diagram showing the overall structure of the QIR algorithm.

failure of this product to match the joint probability distribution function (PDF) is evidence that band 5 contains information about band 6 not captured by band 7.

The clear distinction between the distributions shown in Figs. 1 and 2 simply illustrates that band 5 radiances provide new information about band 6 not provided by band 7. Similarly, as we add other spatial and spectral variables, we can improve the estimation of band 6. We carefully balance the gain in information with potential overfitting by limiting the model to a multilinear estimator and adjusting the window size according to results obtained on independent test data. The effectiveness of this approach is validated in Section VI.

The outline of the QIR algorithm is presented in the diagram shown in Fig. 3. The damaged band to be restored, for example, band 6 on MODIS/Aqua, is referred to as the “bad band.” The bands which we use in the QIR algorithm as input, bands 1–5 and band 7 in the MODIS/Aqua example, are referred to as “good bands.” The first preprocessing step deals with the fact that there are some scattered pixels in the good bands with missing or out-of-valid-range values.

We start processing the data by attempting to fix out-of-valid-range values because pixels with values outside of the valid range will wreak havoc with regression since good band values provide input for the QIR algorithm. We preprocess out-of-range values using an adaptive mean value filter, which replaces isolated missing pixels with the mean value of the valid pixels in a window with an adaptive size. The adaptive window size is the minimum size such that the majority of the pixels in the window are within valid range. Note that the window is limited to a fixed maximum size. The restoration is aborted if more than half of the pixels in the good bands are bad.

The next step when working with the data is destriping the radiances. As observed in [6], destriping can significantly improve regression. In theory, an image of properly calibrated radiances should not have stripes; nevertheless, some striping artifacts remain and can be removed using histogram specification as is commonly done [4], [5]. We apply destriping to all bands, but if a band’s detectors are well matched so that destriping is not required, then the algorithm essentially returns the unstriped values.

We describe a general QIR algorithm in which we have $K - 1$ good bands and one bad band with broken detectors whose data must be reconstructed. In the case of MODIS/Aqua, we consider all the 250-m bands and all of the functioning 500-m bands as good bands, so we have a total of $K = 7$ bands with 6 good bands. Without loss of generality, we can renumber the bands so that the good bands are numbered 1 through $K - 1$

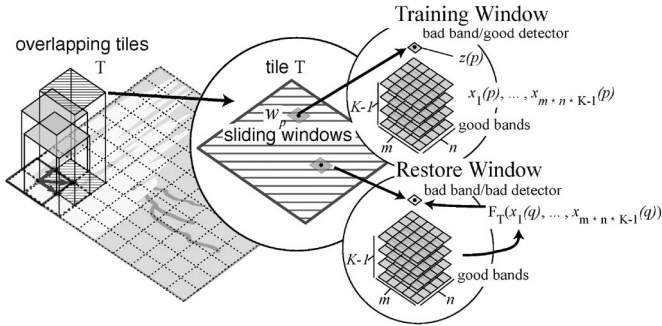


Fig. 4. Diagram showing the process of determining the restoration function for a tile.

and the band to be reconstructed is labeled K . We write the value of a pixel $p = (i, j)$ in the i th scanline (row), the j th column, and the k th band of an image I as $I_{i,j,k}$. This pixel value can be a digital count, radiance, reflectance, or other value type. The QIR algorithm does not depend on the value type and can produce a restoration function that takes inputs and produces output in any of these types.

The restoration function is a composite (piecewise) function built from smaller restoration functions defined on large overlapping portions of the image, which we refer to as *tiles*. The tiles are defined by first partitioning the image into a grid of nonoverlapping tiles, and for MODIS/Aqua, we used 200×200 pixel tiles. The grids of tiles are shifted horizontally by a half tile (100 pixels), vertically by a half tile, and diagonally by a half tile, as shown at the far left of the diagram in Fig. 4. As a result, pixels in a corner region are in only one tile, pixels near the image boundaries but not in corner regions are members of two overlapping tiles, and pixels at least a half tile away from the boundary are covered by four overlapping tiles.

We determine a restoration function independently for each tile. Since a pixel may belong to several tiles, the restored value in the bad band is the average of the independent restoration functions for each tile to which it belongs. For the pixels in the corner regions, the value is determined by the corner tile restoration function, and there is no averaging because there is only a single function. For the other regions, such as pixels away from or near the boundary, a restored pixel value is the average of four or two restoration functions, respectively, one for each tile containing the pixel.

QIR could be generalized to accommodate weighted averages based on distance to the boundary of a tile, but in the MODIS/Aqua case, the extra complexity was unwarranted. We also considered tiles which overlapped by more than half a tile. An extreme case that we considered was using sliding overlapping tiles centered at the band 6 pixel to be restored, providing for a per-pixel varying restoration function. In this case, it might not even be necessary to average restoration functions and could potentially improve accuracy, but it is very expensive when compared to half-tile overlaps. Training data are used to empirically find a balance between accuracy and speed when setting the tile size and the overlaps between the tiles.

For each pixel from a scanline with a broken detector in band K , the restoration function F must provide a value $I_{i_0, j_0, K} =$

$z(q)$, with $q = (i_0, j_0)$, where we think of $z(q)$ as the dependent variable. For each pixel q , the independent variables are taken from the values in the image I for an $m \times n$ spatial window, w_q centered at q , with m and n odd, as shown in Fig. 4. The $m \cdot n \cdot (K - 1)$ independent variables of w_q are

$$\begin{aligned} \mathbf{x}(q) &= \{x_0(q), \dots, x_{m \cdot n \cdot (K-1)}(q)\} \\ &= \{I_{i,j,k}\}_{|i-i_0| \leq \frac{m-1}{2}, |j-j_0| \leq \frac{n-1}{2}, 1 \leq k \leq K-1}. \end{aligned} \quad (1)$$

To determine F , we separately and independently determine an F_T for each tile T . We do this by first collecting a training set made up of the set of independent and dependent values $\{\mathbf{x}(p), z(p)\}_{p \in V_T}$, with V_T being the set of all pixels p corresponding to working detectors in the bad band, as shown at the top right of Fig. 4. This is indicated in Fig. 3 as the box “True Band 6 Value” which is $z(p)$ and as the box “Windows in Bands” which is the variable $\mathbf{x}(p)$ for the window w_p . Every per-tile restoration function $F_T(\mathbf{x}(p))$ has a training error defined as

$$Error(F_T) = \sum_{p \in V_T} |F_T(\mathbf{x}(p)) - z(p)|^2. \quad (2)$$

To determine F_T , we would like to find a function which minimizes this error without overfitting the training set F_T . We partially address the overfitting issue by restricting F_T to one of the simplest possible families of functions, i.e., multilinear functions of the form

$$F_{T,\alpha}(\mathbf{x}(p)) = \sum_t \alpha_t x_t(p) \quad (3)$$

where $\alpha = (\alpha_1, \dots, \alpha_{m \cdot n \cdot (K-1)})$. Therefore, for our implementation of the QIR algorithm, we determine F_T by optimizing for parameters α_t that minimize the training error $Error(F_T)$ [defined in (2)]. The optimal solution for α_t is computed using a least squares solver to obtain the per-tile multilinear regression illustrated by the box at the top right of Fig. 3.

QIR for a pixel q in band K (band 6/Aqua) for a damaged detector proceeds by first determining the tile T containing q . The per-tile multilinear estimator F_T is then applied to the associated window w_q to obtain $F_T(w_q)$, which is the per-tile reconstruction of $\tilde{z}_T(q)$ for the pixel q in band K , as shown in Fig. 4. Finally, as stated previously, the restored value for q , $\tilde{z}(q)$ in the bad band is the average of the per-tile values $\tilde{z}_T(q)$ that contain q . This is indicated as the box “Reconstructed Band 6 Value” in Fig. 3.

Note that, in the QIR algorithm, pixels corresponding to functioning band K (band 6) detectors help determine the multilinear estimators F_T but are not inputs to those estimators. In other words, none of the input values $\mathbf{x}(q)$ for $F_T(\mathbf{x}(q))$ come from band 6, so the only way that the band 6 values from the good detectors influence the value of $F_T(\mathbf{x}(q))$ is through the determination of the parameters α in the large tile T .

We considered extending QIR so that pixel values which are in the bad band but corresponding to good detectors within the spatial window w_q would also be used as input values to F_T . Unfortunately, this is problematic for Aqua since the

pattern of good and bad detectors within the sliding window changes depending on the scanline of the pixel q , so instead of having a single training set V_T , we would need to have a different training set for each configuration and multiple restoration functions F_T for each tile. This reduction in the number of examples per training set results in overfitting and poorer estimation, so we did not take this approach. For other satellites, with a more regular pattern of broken detectors, this approach may be feasible.

We also note that we have used multilinear regression. This may easily be generalized to a polynomial regression. Even without polynomial regression, the choices of window size and tile size provide the QIR algorithm the flexibility to trade off between improved fitting and generalizability, resulting in better estimation.

IV. ALGORITHM EVALUATION

As mentioned previously, although band 6 MODIS/Aqua has extensive damage, the corresponding band 6 MODIS/Terra is functioning normally. This makes it possible to evaluate QIR by simulating the damage to band 6 MODIS/Aqua on band 6 MODIS/Terra. Our evaluation method compares restored images obtained from applying each of the algorithms on the simulated damaged bands to the original undamaged band 6 MODIS/Terra. The same approach was previously used to evaluate a method to restore band 6 using a cubic polynomial function of the values in band 7 [6], [7].

We compared our restoration with the algorithms of Wang *et al.* [7] and Rakwatin *et al.* [6] as well as to our previous algorithm, presented in [2] which only uses the 500-m bands. It was relatively straightforward to directly implement the polynomial proposed in the paper by Wang *et al.*, while Rakwatin *et al.* graciously provided their code for fair comparison. We chose ten granules with varied terrain containing snow, clouds, mountains, and vegetation in order to challenge all the algorithms. These representative ten granules were also chosen from many others because they could be restored with the prior work implementations without failure. We were unable to run the implementation that Rakwatin *et al.* provided on many granules because it was not robust to the bad data that sometimes appear in the granules. This is only a problem with their implementation, *not* their algorithm. Since we wanted to minimize any modification to their code, we restricted the evaluation to granules on which their implementation ran smoothly.

The result of our evaluation, as seen in Fig. 5, was that all the algorithms do reasonably well. As reported by Rakwatin *et al.* in 2009 [6], their algorithm does consistently and significantly better than that of Wang *et al.* [7], and our algorithm, whether run on just the 500-m bands or with the 250-m bands included, performs better than the other algorithms. When the 250-m bands are included, there is a small improvement in performance. It is interesting to note that, while our restoration is more complex in the sense that we use more bands, it is also less complex in that we use a lower order model (linear versus cubic).

Since we were only able to run the cross algorithm evaluation on ten granules, we wanted to verify that the resulting range

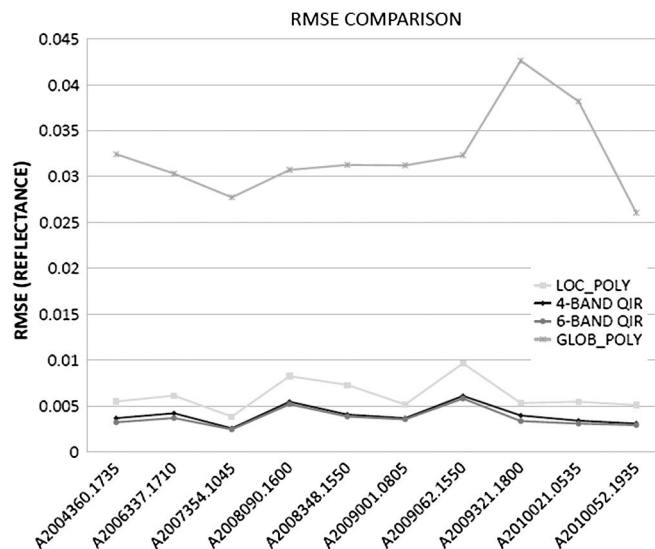


Fig. 5. RMSE, in reflectances, of previous algorithms over ten test granules.

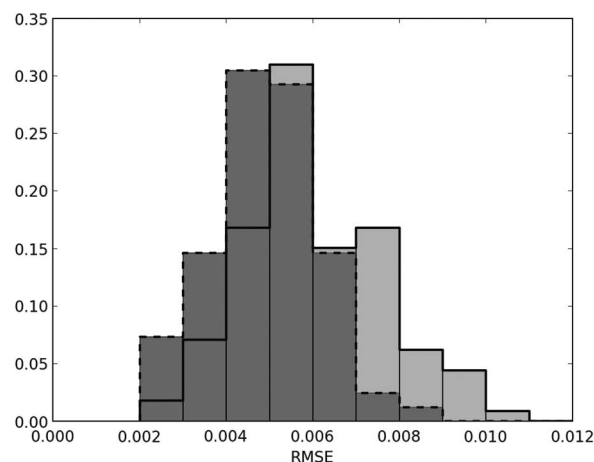


Fig. 6. (Probability) Distribution of the QIR RMSEs in reflectances. These are the errors only for the restored pixels using band 6 MODIS/Terra in which the damage was simulated.

of errors was typical for QIR. To do this, we ran the QIR algorithm on 113 MODIS/Terra granules using just the 500-m bands. We then ran the QIR algorithm on 82 of those granules using all 500- and 250-m bands for restoration; the sample size was reduced because some of the 250-m bands failed the out-of-valid-range preprocessing step. Fig. 6 shows the normalized histogram of root-mean-square errors (RMSEs) for QIR using all the bands (the dashed line) and just the 500-m bands (the solid line). The mean of the 82-granule sample (QIR using six bands) is around 0.004 RMSE, which is consistent with that of the 10-granule sample shown in Fig. 5. The mean RMSE of the 113-granule sample (QIR using only 500-m bands) is slightly higher, which is also consistent with that of the 10-granule sample. The overall improvement when compared to the restoration based on only the 500-m bands is consistent between the smaller and larger samples. We can see, however, that there is a considerable variation in QIR's accuracy depending on the granule. Note that we use reflectances in Figs. 5 and 6 since they were used in prior work [6], [7]. However, the calculation of reflectance uses the solar angle and intensity

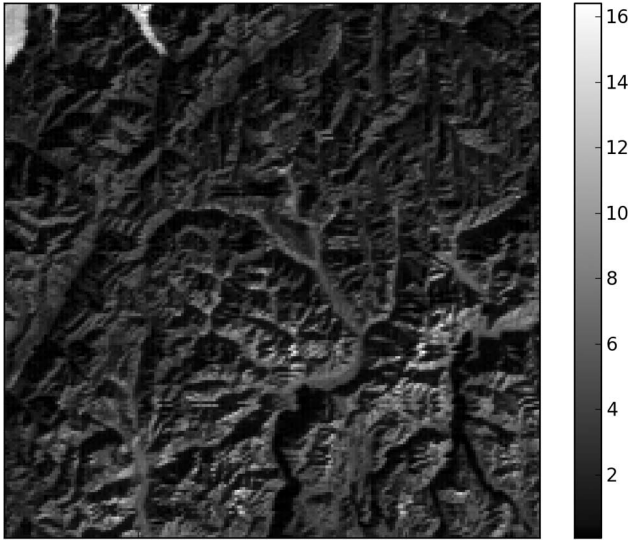


Fig. 7. Image showing band 6 radiances from MODIS on Terra, after simulated Aqua damage and subsequent restoration using QIR.

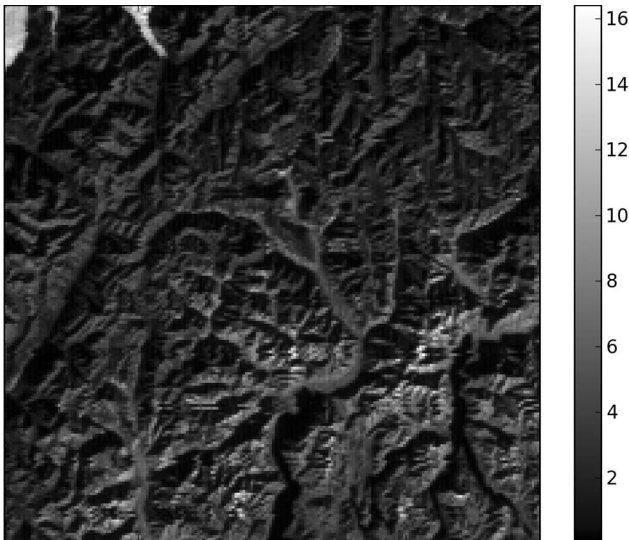


Fig. 8. Image showing band 6 radiances from MODIS on Terra, for comparison with restoration after simulated damage.

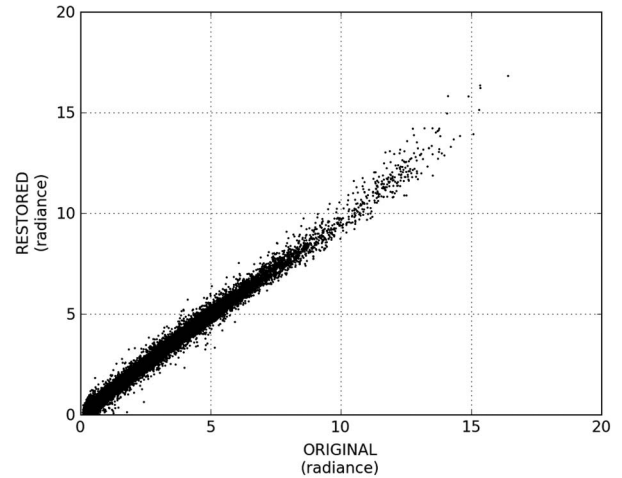


Fig. 9. Scatter plots of band 6 radiances for the patch shown in Fig. 8 to its simulated band 6 shown in Fig. 7.

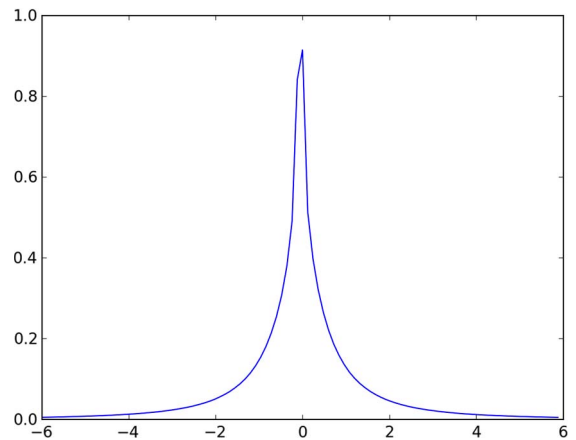


Fig. 10. Probability distribution of errors (differences).

and involves further processing, potentially amplifying or even masking errors in the restoration. Thus, for the remainder of this section, our evaluation will be in units of *radiance*.

In Fig. 7, we show an example of a band 6 MODIS/Terra radiance image that was restored using the QIR algorithm, after first being damaged to simulate band 6 on Aqua. When compared with the original (undamaged) band 6 radiance image (Fig. 8), it is virtually impossible to discern a difference. Using simulated damaged band 6, the scatter plot in Fig. 9 shows how the restored band 6 values compare to the true band 6 values for the same 200-by-200 patch shown in Figs. 7 and 8. The distribution of errors for all of the ten considered granules is shown in Fig. 10. The distribution appears to be far from normal, with many of the errors being quite small.

In the case of MODIS/Aqua, we do not have ground truth available. Still, we can compare QIR to the results that are currently produced with interpolation, shown in Fig. 11. Note

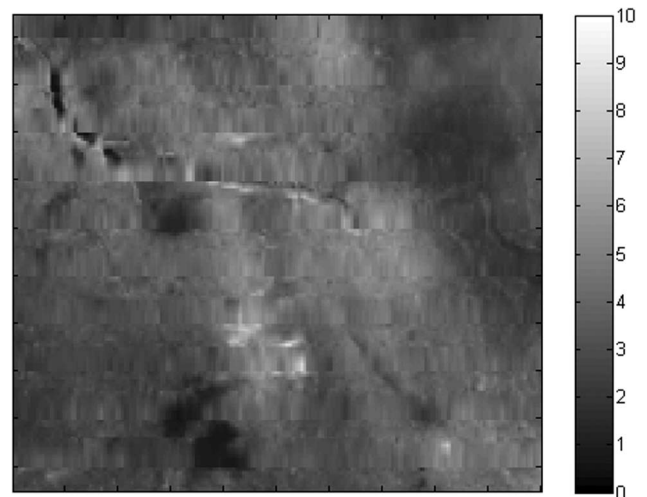


Fig. 11. Detail of band 6 MODIS/Aqua image as published with basic interpolation.

that the river in the interpolated image is completely distorted because columnwise interpolation introduces new edges which completely corrupt spatial derivatives of the image. In contrast,

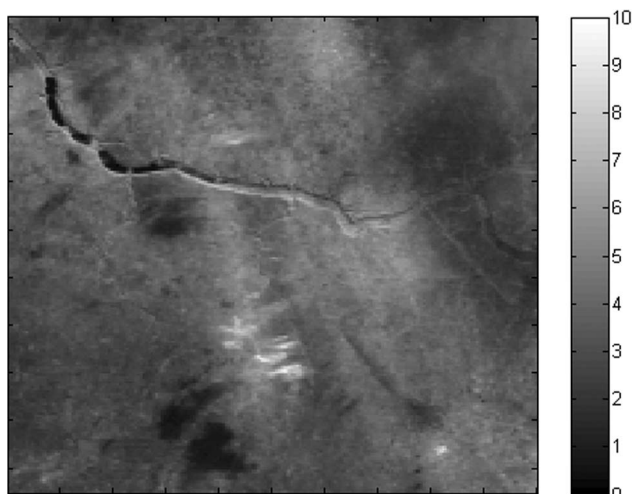


Fig. 12. Detail of band 6 MODIS/Aqua image restored using QIR.

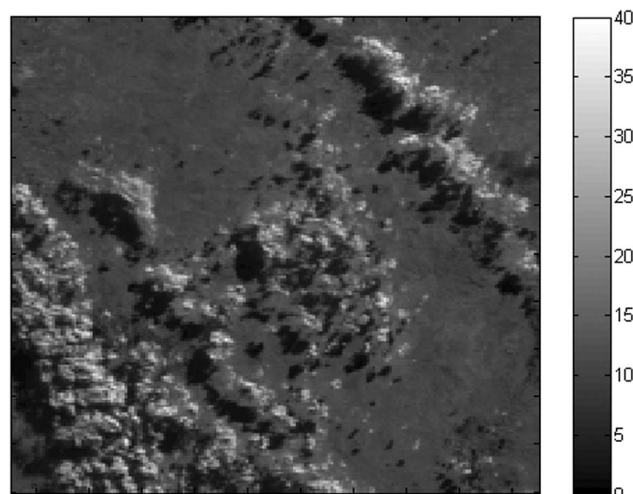


Fig. 14. Detail of a band 6 MODIS/Aqua image restored using QIR.

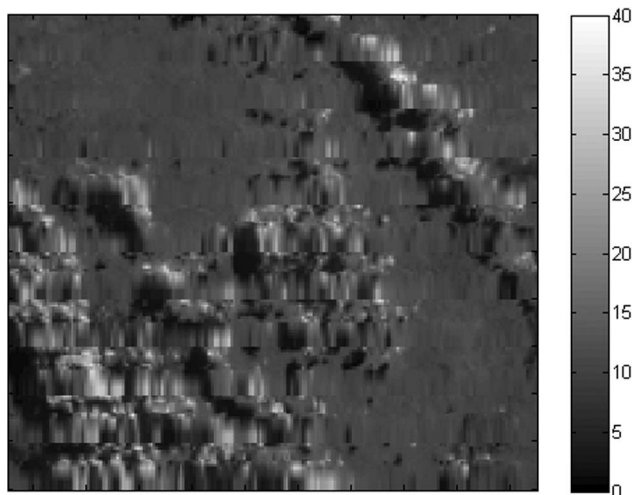


Fig. 13. Detail of a band 6 MODIS/Aqua image with basic interpolation.

the result of QIR in Fig. 12 lacks these strong artifacts. Similarly, we can see that the interpolated image containing many small clouds, shown in Fig. 13, is obviously distorted. There are no obvious artifacts visible in an image produced with QIR, as seen in Fig. 14, and it is even possible to clearly see details like cloud shadows on the ground. The resulting images from our algorithm are high-quality restorations of the damaged bands, both qualitatively and quantitatively.

V. CONCLUSION AND FUTURE WORK

We have presented a general QIR algorithm which uses neighboring pixels, both spectral and spatial, to quantitatively estimate missing values even when the damage to a target band is severe. In the case of MODIS band 6, evaluation shows that our results outperform previous results which were based purely on band 7. We tested across granules with different surface types well separated over time and obtained consistent improvement. We also verified the error rates of our QIR algorithm on the granules that we used to compare with the prior work by using a comprehensive sample of granules.

ACKNOWLEDGMENT

The authors would like to thank P. Rakwatin, W. Takeuchi, and Y. Yasuoka for graciously providing us with the implementation of their restoration algorithm and providing technical advice on how to use it. The authors would also like to thank P. Alabi for helping us process and retrieve data and D. Hall, G. Riggs, and our reviewers for their invaluable suggestions.

REFERENCES

- [1] I. Gladkova, M. Grossberg, and F. Shahriar, "Quantitative image restoration," *Proc. SPIE*, vol. 7695, p. 769 519, 2010.
- [2] I. Gladkova, M. Grossberg, G. Bonev, and F. Shahriar, "A multiband statistical restoration of the Aqua MODIS 1.6 micron band," *Proc. SPIE*, vol. 8048, p. 804 819, 2011.
- [3] [Online]. Available: <http://rapidfire.sci.gsfc.nasa.gov>
- [4] L. Gumley, R. Frey, and C. Moeller, "Destriping of MODIS L1B 1KM data for collection 5 atmosphere algorithms," in *Proc. MODIS Sci. Team Meeting*, Mar. 22–24, 2005. [Online]. Available: http://modis.gsfc.nasa.gov/sci_team/meetings/200503/poster.php
- [5] J. S. Cheng, Y. Shao, H. D. Guo, W. Wang, and B. Zhu, "Destriping MODIS data by power filtering," *IEEE Trans. Geosci. Remote Sens.*, vol. 41, no. 9, pp. 2119–2124, Sep. 2003.
- [6] P. Rakwatin, W. Takeuchi, and Y. Yasuoka, "Restoration of Aqua MODIS band 6 using histogram matching and local least squares fitting," *IEEE Trans. Geosci. Remote Sens.*, vol. 47, no. 2, pp. 613–627, Feb. 2009.
- [7] L. L. Wang, J. J. Qu, X. Siong, H. Xianjun, X. Yong, and C. Nianzeng, "A new method for retrieving band 6 of Aqua MODIS," *IEEE Geosci. Remote Sens. Lett.*, vol. 3, no. 2, pp. 267–270, Apr. 2006.
- [8] C. Ballester, M. Bertalmio, V. Caselles, G. Sapiro, and J. Verdera, "Filling-in by joint interpolation of vector fields and gray levels," *IEEE Trans. Image Process.*, vol. 10, no. 8, pp. 1200–1211, Aug. 2001.
- [9] M. Bertalmio, A. Bertozzi, and G. Sapiro, "Navier-stokes, fluid dynamics, and image and video inpainting," in *Proc. Conf. Comput. Vis. Pattern Recog.*, 2001, vol. 1, pp. 355–362.
- [10] T. Chan, S. Kang, and J. Shen, "Eulers elastica and curvature-based inpainting," *SIAM J. Appl. Math.*, vol. 63, no. 2, pp. 564–592, 2002.
- [11] S. Zhu, Y. Wu, and D. Mumford, "Filters, random fields, and maximum entropy (FRAME): Towards a unified theory for texture modeling," *Int. J. Comput. Vis.*, vol. 27, no. 2, pp. 107–126, Mar. 1998.
- [12] D. Gustavsson, K. Pedersen, and M. Nielsen, "Image inpainting by cooling and heating," in *Proc. Scand. Conf. Image Anal.*, vol. 4522, *Lecture Notes in Computer Science*, B. Ersboll and K. Pedersen, Eds. Berlin, Germany: Springer-Verlag, 2007, pp. 591–600.
- [13] A. Criminisi, P. Perez, and K. Toyama, "Region filling and object removal by exemplar-based image inpainting," *IEEE Trans. Image Process.*, vol. 13, no. 9, pp. 1200–1212, Sep. 2004.
- [14] A. Efros and W. Freeman, "Image quilting for texture synthesis and transfer," in *Proc. SIGGRAPH*, 2001, pp. 341–346.



Irina Gladkova received the B.Sc. degree in mathematics from Donetsk State University, Donetsk, Ukraine, in 1989, the Ph.D. degree in physical/mathematical sciences from the Institute of Applied Mathematics and Mechanics, National Academy of Sciences of Ukraine, Donetsk, in 1993, and the Ph.D. degree in mathematics from The Graduate Center, The City University of New York (CUNY), New York, in 1998.

Since 1998, she has been a Faculty Member with The City College of New York, CUNY, where she is currently an Associate Professor with the Department of Computer Science. She works extensively with engineers and scientists on a variety of applied problems in the area of signal processing. Her main current interests include radar waveform design and satellite data analysis/compression.



Fazlul Shahriar received the B.S. degree with a major in computer science and a minor in mathematics from The City College of New York, The City University of New York (CUNY), New York, in 2010. He is currently working toward the Ph.D. degree in computer science in The Graduate Center, CUNY, with the Chancellor's Fellowship.

He has coauthored several conference papers on satellite image processing.

Mr. Shahriar was a recipient of the Charles Weldon Memorial Award.



George Bonev received the B.Eng. degree in computer engineering and the M.S. degree in computer science from The City University of New York (CUNY), New York, in 2009 and 2011, respectively, where he is currently working toward the Ph.D. degree in computer science in The Graduate Center, CUNY.

He coauthored several conference papers on satellite image processing.



Michael D. Grossberg received the Ph.D. degree in mathematics from the Massachusetts Institute of Technology, Cambridge, in 1991.

He was a Lecturer with the Computer Science Department, Columbia University, New York, where he was also a Ritt Assistant Professor of mathematics. He spent four years as a Research Scientist with the Columbia Automated Vision Environment, Columbia University. He has held postdoctoral fellowships at the Max Planck Institute for Mathematics, Bonn, Germany, and The Hebrew University of Jerusalem, Jerusalem, Israel. He is currently an Assistant Professor of computer science with The City College of New York, The City University of New York, New York. He has authored and coauthored papers that have appeared in International Conference on Computer Vision, European Conference on Computer Vision, and Computer Vision and Pattern Recognition. He has filed several U.S. and international patents for inventions related to computer vision, as well as for multispectral image compression. He has also developed algorithms for medical imaging segmentation and satellite image compression and restoration and is developing a collaborative science system for experiments on high-performance computing facilities. His research in computer vision has included topics in the geometric and photometric modeling of cameras, and analyzing features for indexing.



Peter Romanov received the B.S. and M.S. degrees in physics from Leningrad State University (currently Saint Petersburg State University), Saint Petersburg, Russia, in 1983 and the Ph.D. degree from the Central Aerological Observatory, Moscow, Russia, in 1989.

Between 1987 and 1996, he was with the Hydrometeorological Centre of Russia, Moscow, where he performed analysis of satellite sounding data for meteorological applications. From 1997 to 1998, he was with Universite de Sherbrooke, Sherbrooke, QC,

Canada, where he supervised the Canadian branch of the National Aeronautics and Space Administration's AEROSOL ROBOTIC NETWORK of ground-based sun photometers. Since 1998, he has been a Visiting Scientist with the National Environmental Satellite Data and Information Service, National Oceanic and Atmospheric Administration (NOAA), Camp Springs, MDA. Since 2010, he has been with the NOAA/Cooperative Remote Sensing Science and Technology Center, The City College of New York, The City University of New York, New York. His primary interests include the development of satellite data processing techniques and the application of remote sensing data to monitor Earth's land surface cover.